Nature Communications

https://doi.org/10.1038/s41467-026-76174-3

Article in Press

Staple crops as a key hub of biogeochemical mercury cycle across China

Received: 10 May 2026

Accepted: 22 July 2026

Published online: 29 July 2026

Cite this article as: Wang, Y.-K., Wen, S., Liu, N. *et al.* Staple crops as a key hub of biogeochemical mercury cycle across China. *Nat Commun* (2026). https://doi.org/10.1038/s41467-026-76174-3

Yu-Kun Wang, Shuhai Wen, Nantao Liu, Yun-Yun Hao, Long Chen, Jiao Feng, Yanxu Zhang, Xun Wang & Yu-Rong Liu

Staple crops as a key hub of biogeochemical mercury cycle across China

Yu-Kun Wang[1,2], Shuhai Wen[1,2], Nantao Liu[3], Yun-Yun Hao[4], Long Chen[5], Jiao Feng[1,2], Yanxu Zhang[6], Xun Wang[3*], Yu-Rong Liu[1,2*]

[1]State Key Laboratory of Agricultural Microbiology, Huazhong Agricultural University, Wuhan 430070, China

[2]College of Resources and Environment, Huazhong Agricultural University, Wuhan 430070, China

[3]State Key Laboratory of Environmental Geochemistry, Institute of Geochemistry, Chinese Academy of Sciences, Guiyang 550081, China

[4]National Biopesticide Engineering Research Centre, Hubei Academy of Agricultural Sciences, Wuhan 430070, China

[5]Key Laboratory of Geographic Information Science (Ministry of Education), School of Geographic Sciences, East China Normal University, Shanghai 200241, China

[6]Department of Earth and Environmental Sciences, Tulane University, New Orleans, LA 70118, USA.

***Corresponding authors**

Yu-Rong Liu; E-mail: yrliu@mail.hzau.edu.cn

Xun Wang; E-mail: wangxun@mail.gyig.ac.cn

Abstract

Mercury (Hg) contamination threatens human health and ecological security. Plants play a critical role in regulating the global Hg cycle, yet how agricultural crops influence Hg transport remains elusive. Here we show that staple crops assimilate 25.59 Mg (22.81–27.25 Mg) Hg annually based on a standardized field survey of 301 sites across China, with approximately 53% originating from the atmosphere and 47% from the soil according to Δ^{199}Hg signatures. We further predict the North China Plain, Jiangnan Hills, and Northeast Plain as hotspots of crop Hg accumulation in China. Following harvest, 36.4% of the Hg accumulated by staple crops is returned to the soil as residues, while 43.4% is transferred to the food chain via grain consumption and straw-livestock feed. These findings demonstrate that staple crops act as a key hub in global Hg cycling, with implications for assessing the fate and risk of existing Hg on Earth.

Introduction

Mercury (Hg) is a potent toxic element ranked among the top ten chemicals of major public health concern by the World Health Organization (WHO)[1]. Since the Industrial Revolution, human activities such as coal combustion, gold mining, and cement production have released vast quantities of geologically stored Hg into the atmosphere, leading to a 3- to 5-fold increase of global atmospheric Hg concentrations[2,3,4]. The anthropogenic Hg undergoes long-range transportation via atmospheric circulation and then enters terrestrial ecosystems through wet and dry deposition. As an important biome on Earth, vegetation not only takes up soil Hg through its roots but also assimilates atmospheric Hg via foliar stomata, which is the dominant pathway for dry deposition of atmospheric Hg[5,6]. It is estimated that global vegetation takes up approximately 2,500 Mg of atmospheric Hg annually, and this is comparable to the amount of global anthropogenic Hg emissions[2,7]. This uptake shortens the residence time of atmospheric Hg by 8–10 months[5]. For instance, forests serve as significant Hg sinks, annually transferring 1,180 Mg of atmospheric Hg absorbed through litterfall into the soil[8]. Compared with forests, agricultural crop systems are more closely related to human activities; however, we currently know little about the Hg accumulation by crops and their role in the global Hg cycle.

Unlike the perennial succession of forest vegetation, crops have short growth periods and are heavily influenced by human interventions. Globally, crops provide more than 90% of dietary energy intake[9], and their high biomass turnover under intensive agricultural management may continuously affect Hg cycling. Previous studies have shown that crops absorb atmospheric and soil Hg primarily through their leaves and roots, respectively, resulting in a distinct tissue-specific partitioning[6,10]. Atmospheric Hg absorbed by crops is predominantly stored in aboveground tissues such as leaves and stems, whereas soil-source Hg is largely retained in roots[11,12]. The absorbed Hg can subsequently be translocated to grains during plant growth, increasing the health risk via dietary intake of Hg-contaminated food[13]. Subsequent straw management, whether incorporated into soils[14,15], used as animal feed[14], or open burning[16], allocates the crop Hg to different environmental compartments. Thus, Hg absorbed by crops may influence food safety and Hg cycling through its distribution in edible tissues and subsequent post-harvest management.

As primary sources of global caloric intake, staple crops including wheat, rice, and maize are widely cultivated across hundreds of millions of hectares worldwide, forming an intricate web of Hg bioaccumulation spanning multiple climatic zones. Taking China as an example, wheat, rice, and maize, collectively occupy 84% of the total grain cultivation area[17], representing potential Hg sinks and reallocation hubs. Mercury accumulation in the crops may be influenced by multidimensional variables, including crop parameters (e.g., biomass)[14], Hg sources (e.g., atmospheric Hg deposition, soil Hg)[18], geoclimatic factors (e.g., elevation, CO_2 concentration)[19,20], soil properties (e.g., SOC, texture)[21,22], and management practices (e.g., fertilization, irrigation)[18]. However, the effects of these variables on Hg accumulation in crops and their subsequent fate remain unclear, limiting our understanding of crop contributions to global Hg cycling.

To address these knowledge gaps, we conducted a standardized field survey of 301 sites spanning a 4,630 km transect across China, collecting paired samples of staple crops (i.e., wheat, rice, and maize) and soils. We first determined the total amount of Hg accumulation in the three staple crops by integrating tissue Hg concentrations with measured biomass, and used Hg isotopic compositions to quantify the respective contributions of atmospheric and soil sources to the accumulation. Then, we explored the relative importance of the examined environmental variables for Hg accumulation in staple crops, and applied machine-learning approaches to predict the spatial distribution of crop Hg accumulation based on their associations. Furthermore, using publicly available datasets of cereal residues, we evaluated the fate of crop Hg across environmental compartments. This work fills a critical gap in understanding the role of crops in global Hg cycling, and provides valuable data to support the implementation of the *Minamata Convention*.

Results

Mercury accumulation in staple crops across China

Field surveys showed that Hg concentrations in the staple crops (whole plants) ranged from 0.98 to 106.65 ng g^{-1} (average: 13.16 ± 12.69 ng g^{-1}) (Fig. 1A), with values peaking in subtropical regions (average: 16.44 ± 14.65 ng g^{-1}) (Supplementary Fig. 1). Consistent with higher Hg concentrations in rice than in wheat and maize (Fig. 1A), paddy soils had the highest Hg concentrations (Fig. 1B). Moreover, crop Hg concentrations were significantly positively correlated with that of the soil (Supplementary Fig. 1). Despite variations in Hg concentrations among crops, the Hg accumulation per unit area was comparable, with an average of 25.70 μg m^{-2} (Fig. 1C). Consequently, Hg accumulation in the three staple crops was estimated to reach 25.59 Mg (22.81–27.25 Mg) annually in China, with wheat, rice, and maize contributing 5.77 Mg (4.60–7.07 Mg), 8.68 Mg (7.09–8.99 Mg), and 11.14 Mg (9.73–13.04 Mg), respectively (Fig. 1D; Supplementary Fig. 2). Further isotopic analysis showed that the Δ^{199}Hg signatures of atmospheric Hg^0, soil, and whole-plant crop samples were 0.10 ± 0.05‰, −0.08 ± 0.04‰, and 0.01 ± 0.04‰, respectively (Supplementary Fig. 3). Based on these Δ^{199}Hg signatures and a Hg isotope mixing model, we estimated that the atmosphere contributes approximately 64% of the Hg in maize, which is higher than the corresponding contributions in wheat and rice. Overall, approximately 53% (52.1–53.9%) of the Hg accumulated in these crops originated from the atmosphere, while the remaining 47% (46.1–47.9%) was derived from the soil (Supplementary Fig. 3; Supplementary Fig. 4).

Key factors influencing Hg accumulation in staple crops

Variance-based relative importance analysis revealed that vegetation parameters and Hg sources explained a greater share of variability in crop Hg accumulation than geoclimatic factors, soil properties, or anthropogenic factors (Fig. 2A-C). Specifically, crop biomass, soil Hg, and gaseous elemental Hg deposition (Hg^0_dep) accounted for 22.6–33.7%, 6.6–24.4%, and 5.2–9.8% of the total variance, respectively (Fig. 2A-C). Consistently, Hg accumulation in staple crops was positively correlated with Hg^0_dep and crop biomass (Supplementary Fig. 1). Crop-specific environmental associations were also observed. For example, wheat and rice Hg were positively correlated with soil Hg, and rice and maize Hg accumulation was positively correlated with SOC (Supplementary Fig. 1). Further analyses of Structural Equation Modeling (SEM) indicated that Hg sources and crop biomass exerted direct positive effects on Hg accumulation across the three crops (Fig. 2D-F; Supplementary Fig. 5). Climatic factors and soil properties affected Hg accumulation indirectly by influencing the primary drivers (i.e., Hg sources and crop biomass).

Specifically, atmospheric CO_2 concentration promoted Hg accumulation through its effects on Hg^0_dep, and mean annual temperature (MAT) promoted wheat Hg accumulation by enhancing both Hg^0_dep and soil Hg (Fig. 2D-F). Differently, solar radiation (SRAD) suppressed rice Hg accumulation by affecting Hg^0_dep, while SOC and clay content promoted rice Hg accumulation by adsorbing soil Hg (Fig. 2E).

Hotspots for Hg accumulation in staple crops

Based on the associations between crop Hg and selected variables, we predicted the spatial distribution of crop Hg accumulation using the extremely randomized trees algorithm (ERT), which outperformed other candidate algorithms in 10-fold cross-validation (Supplementary Fig. 6). Results revealed substantial spatial heterogeneity in Hg accumulation in staple crops across China (Fig. 3). The subtropical, warm temperate, and mid-temperate zones account for the majority of staple crop Hg accumulation (Supplementary Fig. 7). Within these zones, the Jiangnan Hills, North China Plain, and Northeast Plain together account for 60.2% of the total amount of Hg accumulation in China (Supplementary Fig. 7). Specifically, the Jiangnan Hills, North China Plain, and Northeast Plain accounted for 24.6%, 71.5%, and 36.5% of the Hg loads for rice, wheat, and maize, respectively (Fig. 3). Notably, these geographic hotspots with high amounts of Hg accumulation are spatially distinct from the predicted high-concentration zones centered on the Yunnan-Guizhou Plateau in Southwest China (Supplementary Fig. 8).

Multi-pathway flow of Hg in staple crops across China

As detailed in Methods, we combined the estimates of Hg accumulation in staple crops with a crop-residue dataset and estimated that staple crops in China introduce approximately 11.12 Mg (9.84–11.85 Mg) of Hg into the food chain annually (Fig. 4A). Of this total, harvested grain accounts for 4.74 Mg (4.46–5.23 Mg), with rice alone contributing 2.56 Mg (2.33–2.99 Mg) (Supplementary Fig. 9; Supplementary Fig. 10). Straw used as livestock feed constitutes another critical pathway, transferring 6.38 Mg (4.87–7.19 Mg) of crop Hg into the food chain each year (Supplementary Fig. 9; Supplementary Fig. 10). Meanwhile, an estimated 9.30 Mg (8.30–9.97 Mg) of crop-derived Hg is returned to soils via straw incorporation and root retention (Fig. 4B; Supplementary

Fig. 10), and open burning and other uses (e.g., household fuel, mushroom cultivation substrate) represent 8.7% (8.4–9.5%) and 11.5% (10.9–11.8%) of the total amount of accumulated Hg, respectively (Fig. 4C-D; Supplementary Fig. 10). Notably, Hg emissions from burning wheat residue alone amount to 1.12 Mg (0.89–1.37 Mg), equal to the combined total from burning rice and maize residues (Fig. 4C; Supplementary Fig. 9; Supplementary Fig. 10).

Discussion

Agricultural crops are typical anthropogenic vegetation and are posited to play a potential role in regulating the global Hg cycle. While crops are known for high biomass turnover rates and significant involvement in the cycling of elements such as carbon and nitrogen[23], knowledge regarding the role of crops in Hg turnover remains limited. Through large-scale field surveys of staple crops across broad environmental gradients, this study quantifies Hg accumulation in crops and predicts the distribution and subsequent fate of accumulated Hg, thereby identifying the role of agricultural ecosystems in global biogeochemical Hg cycling.

Mercury accumulation per unit area in staple croplands exceeds that reported for temperate forests (12.4-26.2 μg m^{-2} yr^{-1})[24]. Accordingly, the amount of Hg accumulated annually in staple crops is equivalent to the annual sequestration by approximately 59 million hectares of temperate forest, an area approaching 25% of the total forest cover of China. These results underscore the significant capacity of staple crops to mobilize environmental Hg. As integrators of atmospheric Hg deposition and soil Hg pools, crop systems in China accumulate an annual Hg mass comparable to the litterfall-mediated input to forest soils (27 Mg yr^{-1})[25]. Unlike in forests, the Hg accumulated in crop biomass remains in active circulation through grain consumption and residue management (Fig. 5), positioning crop systems as dynamic nodes rather than passive sinks in regional Hg budgets. Remarkably, the amount of Hg taken up by staple crops across China matches the scale of emissions from the key industrial sector of iron and steel production (25.5 Mg yr^{-1})[26]. Therefore, we argue that crop systems should be recognized as an active and major contributor to regional and global Hg budgets.

This hub function arises from the strong capacity of crops to directly couple atmospheric and soil Hg pools. Our isotope evidence confirms that Hg accumulation in staple crops relies heavily on both foliar stomatal uptake from the atmosphere and root uptake from the soil (Supplementary Fig. 3), distinct from forest ecosystems where Hg accumulation is largely governed by atmospheric Hg^0 deposition[7,27]. This disparity is largely driven by agricultural management practices. In general, long-term irrigation and fertilization enrich agricultural soils with Hg, making the soil-root pathway a critical contributor to crop Hg accumulation, particularly in flooded rice paddies[11,28,29], which is also corroborated by our observation of a higher proportion of soil-derived Hg in rice compared to dryland crops (Supplementary Fig. 3). Collectively, this dual-source assimilation enables crop systems to function as effective transfer hubs that integrate Hg from both atmospheric and edaphic reservoirs.

Hub strength is further regulated by biological and environmental drivers. In farmlands, highly variable biomass associated with intensive cropping appears to drive crop Hg accumulation, agreeing with the results of relative importance analysis, SEM, and Shapley additive explanations (SHAP) (Fig. 2; Supplementary Fig. 5; Supplementary Fig. 11). In forests with limited annual biomass increment, however, Hg accumulation is more sensitive to factors controlling uptake efficiency, such as evapotranspiration[27]. Within cropland systems, climatic factors could influence hub efficiency through crop stomatal conductance. For instance, elevated CO_2 concentrations may enhance atmospheric Hg uptake through increasing stomatal conductance associated with photosynthetic fertilization[30], despite possible inhibitory effects under higher CO_2 levels[31]. These responses reflect species-specific physiological regulation and non-linear sensitivities to elevated CO_2 concentrations. Similarly, higher MAT may promote Hg uptake in wheat by facilitating leaf stomatal opening[32,33,34]. It should be noted that strong SRAD could restrict Hg^0 uptake in rice by inducing partial stomatal closure under intense light[35]. In addition, soil properties primarily influence the soil-to-crop transfer pathway within this hub. For example, SOC binds strongly to Hg^{2+}, and clay minerals with large surface areas adsorb Hg through oxygen-containing functional groups (e.g., hydroxyl and carboxyl groups), which jointly enhance the retention of Hg in soils[36]. In hypoxic flooded rice paddies, a portion of this retained Hg may be converted into more bioavailable methylmercury by microorganisms, increasing Hg accumulation in rice[37,38]. These results indicate that crop Hg accumulation is jointly regulated by source strength, biomass production, and environmental controls.

The interplay of the aforementioned mechanisms with the local environment and agricultural management gives rise to pronounced spatial heterogeneity in crop Hg accumulation, reflecting spatial variability in hub strength. It should be noted that spatial patterns of total Hg accumulation and Hg concentration are not necessarily consistent across regions, because total accumulation is jointly controlled by both crop Hg concentration and biomass production. Therefore, areas with relatively high Hg concentrations do not always correspond to the largest accumulation hotspots if crop productivity is limited. For example, despite the high geological Hg background in the Yunnan-Guizhou Plateau, crop Hg accumulation remains relatively low, which is consistent with the fact that the combined staple crop planting area of Yunnan and Guizhou accounts for only 5.6% of the total crop planting area in China[17], a pattern associated with traditional, small-scale, decentralized agricultural practices shaped by mountainous terrain and diverse ethnic farming customs[39,40,41]. In the subtropical Jiangnan Hills, millennia of rice cultivation have made rice the staple food for inhabitants of densely clustered rural villages[42]. The long-term coexistence of intensive rice cultivation with industrial Hg emissions from sources such as non-ferrous metal mining, coal-fired power plants, and cement production has significantly enhanced Hg fluxes in cropping systems[43], highlighting the conflict between securing staple food supplies and mining-related pollution in resource-dependent rural economies. The Northeast China Plain features policy-supported, large-scale production on fertile black soils[44], resulting in high crop Hg accumulation due to large biomass production, despite relatively low Hg concentrations in individual crops. The North China Plain represents a typical warm-temperate crop-producing region, where industrial legacies and large-scale intensive cultivation of wheat and maize lead to significant Hg accumulation. Owing to the “north-to-south grain transfer” policy[45], this accumulated Hg may undergo extensive spatial displacement through grain trade. Grain trade not only facilitates cross-regional Hg redistribution[46,47], but also encapsulates the role of crop systems as active hubs that bridge and redistribute disparate geographical Hg pools.

The functional significance of this hub role is further underscored by its efficiency in exporting accumulated Hg into biological and environmental reservoirs. It is estimated that 18.5% (17.79–20.99%) of the Hg accumulated in these crops enters the human food chain via harvested grain every year, with rice contributing more than half of this exposure in China. A previous study suggested that methylmercury accounts for approximately 30.9% of the Hg accumulated in rice grains[48]. Given its high toxicity and bioavailability, this speciation strengthens the coupling between Hg biogeochemical cycling and human exposure in rice-dominant regions such as the Jiangnan Hills[49]. The amount of Hg entering the food chain via straw used as livestock feed exceeds that from harvested grain, thereby creating an indirect exposure pathway to humans through animal products such as meat and milk. This identifies crop residues as a critical, yet often overlooked, node in the redistribution of Hg within regional food systems. Additionally, Hg returned to farmland soils through root residues and straw incorporation constitutes a fresh and more bioavailable soil Hg source[50]. In rice paddies, this Hg can be methylated by soil microorganisms into highly neurotoxic methylmercury, which is then absorbed by rice plants and translocated into grains, forming a "soil-rice-food chain" exposure cycle[22]. In subtropical regions, higher temperatures and increased precipitation accelerate rice straw decomposition[51], promoting Hg release from straw into the soil. Together with multi-season cropping practices, these conditions further intensify this cycle. Moderate straw return can also enhance carbon sequestration and amplify Hg accumulation in crops[52,53]. Moreover, open burning of crop residues after harvest releases Hg accumulated during the growth season, leading to regional atmospheric Hg pollution, particularly in wheat-growing areas. This is largely because a higher proportion of wheat straw is burned to secure the planting window for subsequent crops compared with rice and maize straw[54]. Nevertheless, Hg remobilization via this pathway could be effectively constrained by strict implementation of the ban on crop residue burning since 2014[55]. Mercury from other uses (2.94 Mg yr^{-1}) (2.60–3.07 Mg yr^{-1}) has a more complex fate due to a lack of constraining data (Fig. 4D; Supplementary Fig. 10), which may be emitted into the atmosphere as household fuel, volatilized or entered into farmland via composting, or transferred to mushrooms as mushroom cultivation substrate and then into the human food chain[56,57]. Our scenario analysis further suggests that residue management offers practical opportunities for Hg mitigation, but with clear trade-offs (Supplementary Fig. 12). Banning open burning would reduce atmospheric Hg re-emission from 2.23 Mg yr^{-1} to zero, whereas reallocating the straw otherwise burned to field incorporation or livestock feed would increase Hg inputs to cropland to 11.53 Mg yr^{-1} or Hg fluxes into the food chain to 13.35 Mg yr^{-1}, respectively. Although using straw as livestock feed may provide economic benefits, diverting all straw to livestock production would increase Hg entering the food chain from 11.12 to 20.96 Mg yr^{-1}, posing potential risks to human health. Similarly, returning all straw to fields would lead to 20.85 Mg of Hg being incorporated into agricultural soils. Continuous annual straw return would exacerbate long-term Hg accumulation in soils across successive growing seasons. Thus, no single residue management strategy can minimize all Hg risks simultaneously, as such measures only redistribute rather than eliminate crop-derived Hg. In practice, mitigation should be tailored to local Hg background levels and management capacity: in areas with elevated soil Hg background, the proportion of residues returned to fields should be reduced or carefully regulated to limit additional Hg re-input; by contrast, residues with relatively low Hg concentrations may be preferentially directed to livestock feed or other controlled resource-recovery uses, provided that residue Hg concentrations meet relevant safety standards and downstream transfers are properly managed. Effective mitigation requires not only pathway-specific controls, but also careful management of diverted residues to avoid shifting Hg burdens among environmental compartments. Taken together, these migration pathways indicate that, under the combined influence of climate and human activities, staple crop systems function not merely as passive receptors, but as active biogeochemical nodes that integrate, transform, and redistribute Hg across the atmosphere, pedosphere, and biosphere.

The hub role of crop systems represents a globally relevant but underappreciated component of the Hg cycle. Relative to natural vegetation, managed croplands exert distinct controls on Hg residence time and cross-compartment redistribution through crop uptake, harvest removal, and residue management. Large-scale land-use changes, such as deforestation and cropland expansion in regions like the Amazon Basin, may also enhance Hg mobilization by increasing biomass turnover, soil disturbance, and human-mediated redistribution[58]. These processes imply that agricultural expansion may intensify Hg cycling, rather than merely redistribute Hg across land surfaces. However, most existing

Hg assessment frameworks do not explicitly represent cropland-specific processes (e.g., irrigation, fertilization, residue return, multi-cropping, and harvest removal), leaving their effects on Hg retention and redistribution poorly constrained within large-scale assessment frameworks, and potentially contributing to uncertainties in regional and global Hg budgets[31,59]. In this context, our study provides not simply another regional inventory, but empirical constraints on crop uptake and its key regulatory drivers, together with source partitioning, biomass-linked accumulation, and residue-mediated redistribution. These constraints can support the evaluation and future refinement of terrestrial Hg model components, especially in regions where croplands occupy a substantial fraction of the land surface. Recognizing crop systems as active hubs that integrate and redistribute Hg among the atmosphere, soils, and food systems is therefore essential for improving assessment frameworks and reducing projection uncertainties under future climate and land-use change. More broadly, our findings advance the conceptual view of croplands from passive receptors of contamination to managed ecosystems that can substantially reshape Hg dynamics across environmental and biological compartments.

Several uncertainties and limitations should be considered when interpreting these findings. Although we deliberately sampled crops at the late grain-filling stage to characterize the near-final Hg accumulation status of staple crops, and this strategy was supported by comparable Hg levels measured in maturity-stage samples from approximately 25% of sites (Supplementary Fig. 13), our field survey was restricted to 2024 only. This limits our ability to resolve interannual variability in crop Hg accumulation and post-harvest redistribution. In addition, because sampling was conducted across China from April to November to match local crop phenology, residual uncertainty associated with seasonal variation in environmental conditions and atmospheric Hg deposition cannot be fully eliminated. The observed variability in crop Hg concentrations also reflects substantial spatial heterogeneity among sampling sites, driven by differences in climate, precipitation, soil properties, agricultural practices, and atmospheric Hg deposition across diverse agricultural regions. Therefore, multi-year repeated sampling and cross-year comparisons are required to better constrain the temporal dynamics of crop Hg cycling under ongoing climate change, which can be facilitated via cross-regional collaboration and standardized sampling protocols. Our sampling was also restricted to locally dominant commercial crop varieties, which may introduce unquantified uncertainty. Variations in biomass traits and Hg uptake efficiencies across different cultivars may bias national Hg flux estimates and source apportionment results for atmospheric and soil-derived Hg. Moreover, our study focused on three staple crops (i.e., wheat, rice, and maize) across typical cropland systems of China, which may limit generalization to other crop species and habitat environments. While the flux magnitudes reported here are specific to China, processes identified in this study, including dual atmospheric and soil Hg inputs, biomass-linked accumulation, and post-harvest redistribution associated with residue management, may also be relevant in other major agricultural regions, such as rice-growing areas elsewhere in Asia, rapidly expanding agricultural regions in Africa, and intensively managed croplands in the United States. However, their relative importance and quantitative impacts should be evaluated using region-specific observations and management data. Heavily polluted sites were excluded to represent background agricultural conditions, which may lead to underestimation of Hg accumulation in contaminated regions. Furthermore, although a bottom-up approach was employed, the Hg accumulation estimates based on regional survey averages could be refined by incorporating more field samples. Because the Hg budget was based on official annual sown area statistics, regional cropping intensity was implicitly accounted for, but uncertainty may still arise from differences in local cropping practices and the use of provincial-average accumulation values. Inherent limitations related to algorithm suitability, along with uncertainties in raster-based environmental covariates and crop residue datasets, also contribute to overall uncertainty, although multi-model comparisons were employed to mitigate this and intrinsic model uncertainties were quantified (Supplementary Fig. 14).

In summary, this study demonstrates that staple crop systems constitute a significant and active component of the global Hg cycle, with Hg accumulation magnitudes comparable to key industrial emissions and forest sequestration capacities. Crucially, crops accumulate atmospheric and soil Hg within distinct hotspots, including geogenic, industrial-legacy, and biomass-dominated regions, and subsequently facilitate the entry of this Hg into human food chains and environmental reservoirs through grain consumption and residue management. These findings highlight that crop systems are not passive Hg sinks but dynamic Hg transfer hubs, necessitating their integration into global Hg budgets and mitigation strategies. Although derived from China, our results provide empirical evidence for a broader process framework in which intensively managed croplands couple atmospheric deposition, soil Hg pools, biomass production, and post-harvest redistribution. Thus, this study offers a transferable process perspective for evaluating cropland Hg dynamics in other agricultural regions. The hotspot patterns identified here may therefore serve as a process-based reference, rather than a direct spatial template, for other rapidly industrializing and coal-dependent regions. Nevertheless, their temporal stability and cross-regional applicability require further validation, necessitating long-term observational data to track the impacts of high-accumulation crops like rice and critical transfer pathways such as residues used for livestock feed on the Hg cycle. Concurrently, it is imperative to quantify how agricultural management, climate change, and policy actions such as the *Minamata Convention* influence the function of crops as Hg hubs, which will facilitate the design of targeted mitigation strategies to safeguard human and ecosystem health.

Methods

Field survey and laboratory experiments

Sample collection. To obtain reliable data on crop Hg, paired crop plant and soil samples were collected from 301 typical croplands across 29 provinces in China between April and November 2024 (Fig. 1D). Sampling was conducted during the late grain-filling stage of staple crops to avoid biomass loss from leaf senescence at maturity, as both biomass and Hg accumulation are relatively high during this period[60]. Comparison with samples collected at maturity showed consistent Hg accumulation between the two stages (Supplementary Fig. 13), confirming that sampling during the grain-filling stage reliably captures the maximum Hg accumulation in crops. Because China spans multiple climate zones, crop phenology varies substantially among regions. The extended sampling window from April to November 2024 was therefore necessary to collect locally dominant staple crops at a comparable late grain-filling stage across the national survey area, rather than on the same calendar date. This design minimized bias arising from differences in crop developmental stage and improved interregional comparability. To minimize local pollution, all sites were situated at least 5 km from industrial or mining areas. The sampling network spanned longitudes from 77.24°E to 134.00°E and latitudes from 18.56°N to 51.68°N, covering all major staple crop production regions in China. These sites spanned tropical, subtropical, temperate, mid-temperate, and cold-temperate zones, with MAT ranging from −1.4 °C to 25.5 °C, mean annual precipitation (MAP) from 74.6 mm to 2370.8 mm, and elevations from 1 to 2644 m. Within each selected 10 m × 10 m cropland plot, surface soils (0–15 cm) were collected from the four corners and the center of each plot and then combined to form one composite soil sample. At the corresponding soil sampling points, 40 wheat plants, 40 rice plants, or 5 maize plants were collected to match the paired soil samples. All crops were sampled as intact whole plants. To collect intact root systems, we dug around each plant to a sufficient depth to allow complete retrieval of all attached roots with minimal breakage. For wheat and rice, whole plants include roots, stems, leaves and grains, while whole maize plants comprise roots, stems, leaves, grains, cobs and tassels. The geographic coordinates of each sampling site were recorded, and all soil and plant samples were immediately placed on dry ice and transported to the laboratory within 48 h for subsequent analyses. Sampled crops represented the locally predominant varieties to ensure regional representativeness. Provinces with a staple crop cultivation area of less than 0.2% of the total in China were excluded.

To explore the source contributions of Hg in crop plants, four representative sites per staple crop (wheat, rice, and maize) were selected to span major production regions and geographic-climatic gradients (e.g., temperate to subtropical, irrigated plains to arid zones), yielding 12 sites for Hg isotope analysis (Supplementary Fig. 3). Wuhan, located in the middle Yangtze Plain, was included as a mixed-cropping site to enable within-site comparison among the three crops. At these sites, atmospheric gaseous elemental Hg (Hg^0) was collected from grain-filling to maturity stages alongside paired soil and plant samples. The atmospheric Hg^0 was trapped using chlorine-impregnated activated carbon tubes fitted with upstream particulate filters, with air drawn through the tubes at 3 L min^{-1} to enrich Hg^0 onto the activated carbon[61]. The inlet for atmospheric Hg^0 sampling was positioned at 1.2 m above the ground in wheat and rice fields, and at 1.8 m in maize fields, consistent with the respective canopy heights. Quality assurance and quality control protocols for atmospheric Hg^0 sampling followed previously reported studies[62,63].

Determination of crop Hg concentrations and biomass. After transport to the laboratory, crop roots were rinsed sequentially three times with ultrapure water (30 s per rinse) until no visible sediment remained in the water. This standardized procedure completely removes adhering soil particles to prevent artificial overestimation of root Hg concentrations, while avoiding excessive leaching of intrinsic Hg within plant tissues. This identical washing protocol was uniformly applied to wheat, rice and maize, ensuring residual soil contamination would not distort plant Hg data or the subsequent calculation of soil Hg contribution ratios. Plant samples used for Hg determination were then separated into different tissues. Wheat and rice plants were separated into roots, stems, leaves, and grains, whereas maize plants were additionally separated into cobs and tassels. All tissue samples were freeze-dried, finely ground, and sieved to <100-mesh prior to Hg analysis using a DMA-80 direct Hg analyzer (Milestone, Italy) with oxygen as the carrier gas, and each sample was analyzed in triplicate. The detection limit was 0.02 ng Hg based on analyses of empty nickel boats (n = 80). Quality control was conducted using National Standard Reference Materials of China GBW10043a (GSB-21a, rice flour, Hg = 3.5 ± 0.6 ng g^{-1}) and GBW10048a (GSB-26a, celery leaves, Hg = 11.3 ± 1.9 ng g^{-1}), which were analyzed after every 18 samples and yielded recoveries of 85–105%, and the parallel sample error was <10%. For biomass measurement, another set of intact plants (10 wheat or rice plants or 3 maize plants per site) was air-dried to constant weight in 10-mesh nylon bags, and the dry weight of each tissue per plant was then recorded.

Determination of soil pH, SOC, and Hg concentration. After transport to the laboratory, soil samples were cleared of stones and roots, then air-dried and ground. A portion sieved through a 10-mesh sieve was used to determine soil pH in a soil-water suspension (1:2.5 ratio) using a pH meter (Mettler Toledo Instruments Co. Ltd.). Another portion passed through a 100-mesh sieve was used to determine SOC via the $K_2Cr_2O_7$ oxidation titration method and soil Hg content using the DMA-80 direct analyzer, with each sample analyzed in triplicate. Quality control for soil Hg analysis employed reference materials GBW07408a (GSS-8a, soil, Hg = 27 ± 5 ng g^{-1}) and GBW07536 (GSS-45, soil, Hg = 55 ± 5 ng g^{-1}), analyzed after every 18 samples, yielding recoveries of 91% to 105% and parallel sample errors of <5%.

Assessment of crop Hg accumulation

Mercury accumulation was upscaled from crop tissues to provincial and China-scale totals by combining tissue-specific biomass, Hg concentrations, planting density, and cultivation area. For each crop type k (wheat=1, rice=2, maize=3) and tissue j (roots, stems, leaves, grains, etc.), the Hg accumulation in China for that tissue was calculated as follows:

$$H_{j,k} = 10^{-15} \sum_{i} \left(m_{i,j,k} \times c_{i,j,k} \times D_{i,k} \times A_{i,k} \right) \tag{1}$$

where i denotes province; $m_{i,j,k}$ is the dry mass of tissue j per plant (g plant^{-1}); $c_{i,j,k}$ is the Hg concentration of tissue j (ng g^{-1}); $D_{i,k}$ is the planting density (plants m^{-2}); $A_{i,k}$ is the cultivation area (m^2); and 10^{-15} is the unit conversion factor from ng to Mg. The total Hg accumulation of crop k was then obtained by summing across tissues:

$$T_k = \sum_{j} H_{j,k} \tag{2}$$

and the total Hg accumulation of staple crops in China was calculated as:

$$T = \sum_{k=1}^{3} T_k \tag{3}$$

Here, $m_{i,j,k}$, $c_{i,j,k}$, and $D_{i,k}$ correspond to sampling-based measurements, laboratory determinations, and field-collected data. For each province with sampling sites, tissue Hg accumulation per unit area was averaged across all sites. For provinces without sampling data, the China-wide mean of all sites was used. This gap-filling approach may introduce uncertainty because it cannot explicitly capture regional disparities in environmental conditions, Hg sources, agricultural practices, and crop productivity. However, this method was only applied to provinces whose staple crop cultivation area accounts for less than 0.2% of the national total, which substantially reduces the uncertainty imposed on our national-scale Hg accumulation estimates. Provincial totals were obtained by multiplying the unit-area accumulation by the corresponding provincial cultivation area $A_{i,k}$, which was taken from the China Statistical Yearbook 2025[17]. Because sown area reflects the cumulative annual planting area rather than static cultivated land area, it already incorporates regional cropping intensity and multiple harvests in rice-growing regions. The resulting *T* is reported in Mg yr^{-1}.

Δ^{199}Hg-based source apportionment of crop Hg

Mercury in staple crops derives from atmospheric deposition (foliar uptake of gaseous Hg^0) and from soil (root uptake). Advances in stable-Hg isotope techniques allow quantifying the relative contributions of these two pathways. Mercury isotopes undergo both mass-dependent fractionation and mass-independent fractionation (MIF, e.g., Δ^{199}Hg, Δ^{200}Hg, Δ^{201}Hg). Mass-dependent fractionation is produced by most physico-chemical and biological processes and is therefore less diagnostic of source, whereas MIF arises only from specific processes, notably photochemical and magnetic isotope effects, and thus provides a clearer source fingerprint[64]. Odd-mass MIF (e.g., Δ^{199}Hg) is driven mainly by nuclear-volume and magnetic isotope effects. Because these mechanisms are negligible during plant uptake, Δ^{199}Hg in vegetation predominantly records source signatures rather than uptake-induced fractionation. Moreover, the isotope ^{199}Hg has relatively high natural abundance, so Δ^{199}Hg produces larger MIF signals that can be measured more precisely than those of other isotopes and is widely reported in the literature for end-member comparisons[64,65]. Therefore, we used Δ^{199}Hg to estimate the relative contributions of atmospheric Hg^0 (via foliar uptake) and soil Hg (via root uptake) to Hg in crops. Detailed procedures for Hg isotope pre-concentration and measurement are provided in Supplementary Text1. Based on this isotopic framework, we applied a two-endmember mixing model to quantify the relative contributions of atmospheric and soil Hg to each crop type:

$$\Delta^{199}\mathrm{Hg}_{\mathrm{soil,\,k}}\times f_{\mathrm{soil\text{-}veg,\,k}}+\Delta^{199}\mathrm{Hg}_{\mathrm{air\text{-}Hg(0),k}}\times(1-f_{\mathrm{soil\text{-}veg,\,k}})=\Delta^{199}\mathrm{Hg}_{\mathrm{veg,\,k}} \quad (4)$$

where k denotes crop type (wheat, rice, maize); $f_{\mathrm{soil\text{-}veg,\,k}}$ is the fractional contribution of soil-derived Hg to crop k; $\Delta^{199}\mathrm{Hg}_{\mathrm{soil,k}}$ is the Δ^{199}Hg value of the corresponding agricultural soil for crop k; $\Delta^{199}\mathrm{Hg}_{\mathrm{air\text{-}Hg(0),k}}$ is the Δ^{199}Hg value of atmospheric Hg^0 relevant to crop k; and $\Delta^{199}\mathrm{Hg}_{\mathrm{veg,k}}$ is the measured Δ^{199}Hg value of crop k. Accordingly, $(1-f_{\mathrm{soil\text{-}veg,\,k}})$ represents the contribution from foliage uptake of atmospheric Hg^0. The China-scale fractional contribution of soil-derived Hg to Hg accumulated in staple crops ($f_{\text{soil-veg, total}}$) was then calculated as an Hg-accumulation-weighted average across the three crops:

$$f_{\text{soil-veg,total}} = \frac{\sum_{k=1}^{3}(f_{\text{soil-veg,k}} \times T_k)}{T} \tag{5}$$

The China-scale fractional contribution of atmospheric Hg^0 via foliar uptake ($f_{\text{air-veg, total}}$) was calculated by mass balance:

$$f_{\text{soil-veg,total}} + f_{\text{air-veg,total}} = 1 \tag{6}$$

Potential predictors

To predict the spatial distribution of crop Hg accumulation across China, we compiled 32 candidate predictors representing five groups: geoclimatic factors, soil properties, vegetation parameters, Hg-source variables, and anthropogenic factors. Predictor selection was based on mechanistic relevance, literature support, data consistency, and availability of China-wide spatial datasets. All raster layers were harmonized to a common 0.00833° × 0.00833° grid (approximately 1 km at the equator). Details of predictor datasets, raster preprocessing, and the analytical methods (including variance partitioning, relative-importance analysis, correlation analysis, and SEM) are provided in Supplementary Text2. Briefly, we used these approaches to evaluate the relative contributions of predictor groups and individual variables and to identify the dominant environmental controls on crop Hg accumulation.

Model selection and evaluation

Model selection. Machine learning algorithms were employed to capture the complex, nonlinear associations between crop Hg accumulation and various predictors. The entire dataset was randomly divided into ten subsets, following a k-fold cross-validation approach, with nine subsets forming the training dataset and the remaining one used for validation. The coefficient of determination (R^2) from cross-validation served as the performance metric, and the algorithm achieving the highest R^2 value was selected for subsequent prediction. We assessed the performance of eight machine learning models, including ERT, random forest (RF), decision tree (DT), extreme gradient boosting (XGB), support vector machines (SVM), ridge regression (RR), k-nearest neighbors (KNN), and gradient boosted regression trees (GBR), in predicting the distribution of staple crop Hg. Among them, the ERT model achieved the highest R^2 (Supplementary Fig. 6) and was thus selected. A key challenge in regression prediction is to avoid overfitting while maintaining model robustness. The ERT algorithm addresses this by introducing strong randomization during node splitting, where split thresholds are randomly generated instead of calculating the optimal partition. This increases the bias of individual trees slightly, but aggregating a large ensemble of such trees and averaging their predictions substantially reduces the overall variance. Thus, ERT achieves smoother and more accurate predictions of the complex relationships between environmental drivers and crop Hg accumulation. Finally, spatial predictions of crop Hg across China were generated at a 0.00833° × 0.00833° resolution and combined with crop distribution grids to produce the final maps. These maps were projected using the Krasovsky 1940 Albers coordinate system and resampled to a 1 km × 1 km resolution for display.

Feature selection and hyperparameter tuning. Feature selection is crucial for constructing robust models, mitigating overfitting while enhancing performance and interpretability[66]. This study employed a recursive feature elimination (RFE) procedure with hyperparameter optimization at each iteration. Starting with all 32 covariates, feature importance scores guided the sequential elimination process. Within the RFE framework, a nested optimization approach was implemented. Each iteration involved determining the current feature subset and then applying GridSearchCV to optimize five key ExtraTreesRegressor hyperparameters for that specific subset. These included the number of estimators (n_estimators), the maximum tree depth (max_depth), the minimum number of samples required to split an internal node (min_samples_split), the minimum number of samples that must be present in a leaf node after a split (min_samples_leaf), and the proportion of features considered at each split (max_features). Model performance was assessed via 10-fold cross-validation using the R^2 score. Search ranges for these hyperparameters were carefully defined to balance model performance and generalization (Supplementary Table 1). The RFE continued until one feature remained, and the feature subset that yielded the highest cross-validated R^2 was selected as optimal.

This integrated process yielded final feature sets of 11 variables for wheat Hg accumulation model, 13 variables for rice Hg, and 16 variables for maize Hg (Supplementary Table 1). We further calculated the variance inflation factor (VIF) to test multicollinearity among the screened features. No obvious multicollinearity was detected across the three crop-specific feature sets (all VIF values < 5) (Supplementary Fig. 15). Using these final feature sets, we performed a SHAP analysis to quantify the importance of each predictor. SHAP importance is defined as the mean absolute Shapley value, which measures the average marginal contribution of a feature to the model prediction across all possible feature combinations. Thus, a higher mean |SHAP| proportion (mean |SHAP| value for each feature / sum of mean |SHAP| values across all features) indicates greater feature importance (Supplementary Fig. 11).

Independent validation. We added an independent validation using field observations collected in 2025 from selected sampling sites in the North China Plain, Jiangnan Hills, and Northeast Plain (Supplementary Fig. S16). For each validation site, the observed crop Hg accumulation in 2025 was compared with the corresponding 2024 model-predicted value extracted from the mapped raster. This validation was designed to assess the credibility of the identified high-accumulation regions using an independent dataset.

Spatial prediction uncertainty. Prediction uncertainties arose from three primary sources. First, although our sampling sites were widely distributed across major staple crop production regions and covered broad climatic and geographic gradients, the exclusion of industrial areas may limit the generalizability of the model to heavily polluted croplands. Second, discrepancies in the feature data introduced uncertainty, including variations in quality control, noise in grid cells, differing spatial resolution, and inconsistencies in scales. The third source of uncertainty stems from the machine learning methodology itself. Here, we utilized the distribution of predictions from all individual decision trees within the ERT model to calculate the standard deviation for each prediction, which served as a direct metric to quantify the intrinsic uncertainty of the model. Specifically, for each grid cell, the standard deviation of the predictions from all individual trees reflects the stability of the model's estimate at that location. In general, a larger standard deviation value indicates greater disagreement among the trees and hence higher prediction uncertainty. To quantify the uncertainty in crop Hg accumulation hotspot (the North China Plain, Jiangnan Hills, and Northeast Plain), we used the national-scale uncertainty results (Supplementary Fig. S14) to generate hotspot-specific spatial uncertainty distributions (Supplementary Fig. S17). This allowed us to clearly quantify the prediction uncertainty within each hotspot and provided additional support for the reliability of our hotspot delineation.

Generation of final spatial distribution maps

Mapping of crop Hg accumulation across China. Spatial predictions of crop Hg accumulation across China were multiplied by crop distribution raster to generate the final distribution maps. Crop distribution data were used to constrain the spatial extent of each staple crop and to derive crop-specific Hg accumulation patterns. Details on the selection and evaluation of the crop distribution raster are provided in the Supplementary Text3.

Spatial allocation of crop Hg to different utilization pathways. Using the global crop residue dataset from Smerald et al.[56], we averaged per-pixel residue-use proportions over the past five years to produce a straw-utilization-ratio raster, which we resampled and clipped to China using ArcGIS 10.8. Models trained on field-measured data and environmental covariates were then used to estimate per-pixel Hg accumulation in crop tissues (leaves, stems, roots, and grain). We summed the Hg accumulation in aboveground non-grain tissues (leaves and stems) to generate a straw Hg raster (Supplementary Fig. 18), which was multiplied pixel-wise by the utilization-ratio raster to allocate straw Hg to field return, open burning, livestock feed, and other uses. Subsequently, the straw Hg allocated to field return was added to the root Hg raster, representing Hg delivered to soils. Similarly, the straw Hg allocated to livestock feed was added to the grain Hg raster, representing Hg entering the food chain. Given uncertainty about the final fate of maize cobs and tassels, their accumulated Hg was assigned to the "other uses" category.

Assessment of crop Hg fate in China

Given the predefined crop-residue fate pathways, we quantified the Hg amount entering each pathway by combining (i) China-scale Hg pools in different crop tissues and (ii) spatially explicit residue-management fractions[56]. For each crop type k (wheat, rice, maize), straw Hg was first calculated as:

$$\mathrm{Straw}_{\mathrm{Hg},k} = H_{\mathrm{stem},k} + H_{\mathrm{leaf},k} \tag{7}$$

We then estimated how much of $\mathrm{straw}_{\mathrm{Hg,k}}$ flowed into each residue pathway $l \in$ {livestock-feed, return-field, open-burning, other-usages}. Specifically, we used a gridded map of straw Hg, $\mathrm{raster}_{\mathrm{straw\text{-}Hg,\,k}}$ (p), predicted by our models, together with the grid-level pathway fractions $r_{l,k}$ (p) from the crop-residue dataset of Smerald et al.[56], where p denotes grid cells and $\sum_l r_{l,k}(p) = 1$. The China-scale Hg amount entering pathway l for crop k was calculated as an Hg-load-weighted allocation:

$$T_{l,Hg,k} = \mathrm{Straw}_{Hg,k} \times \frac{\sum_p \left(\mathrm{Raster}_{\mathrm{straw-Hg},k}(p) \times r_{l,k}(p)\right)}{\sum_p \mathrm{Raster}_{\mathrm{straw-Hg},k}(p)} \tag{8}$$

This approach converts known pathway fractions into pathway-specific Hg masses, while accounting for the spatial heterogeneity of straw Hg loads. We then summed across crops and combined straw-related flows with tissue-specific Hg pools to obtain China-scale Hg amounts for major fate categories. Mercury entering the food chain was calculated as grain Hg plus Hg in straw used as livestock feed:

$$T_{\mathrm{Hg,food-chain}} = \sum_{k=1}^{3} (H_{\mathrm{grain,k}} + T_{\mathrm{livestock,Hg},k}) \tag{9}$$

Mercury returned to soils was calculated as root Hg plus straw returned to fields:

$$T_{\mathrm{Hg,return}} = \sum_{k=1}^{3} (H_{\mathrm{root},k} + T_{\mathrm{return-field,Hg},k}) \tag{10}$$

Mercury allocated to open burning was:

$$T_{Hg,burning} = \sum_{k=1}^{3} T_{open-burning,Hg,k} \tag{11}$$

and Hg allocated to other uses was:

$$T_{\mathrm{Hg,others}} = \sum_{k=1}^{3} T_{\mathrm{other-usages,Hg},k} + H_{\mathrm{cob,maize}} + H_{\mathrm{tassel,maize}} \tag{12}$$

where maize cob and tassel were added to "others" because they are not included in straw and their final fates are uncertain. We further conducted a simple accounting-based scenario analysis by reallocating the baseline Hg flux among post-harvest pathways to illustrate how alternative residue-management practices may alter Hg recirculation (Supplementary Table 2). Specifically, we evaluated scenarios representing complete elimination of open burning, reduction of straw use as livestock feed, and diversion of residues to field incorporation or other non-burning uses (e.g., composting, mushroom substrate, or household fuel). These scenarios were not intended to predict future adoption, but to provide intuitive policy-relevant contrasts among burning control, enhanced straw return, and reduced livestock-feed use.

Uncertainty quantification using bootstrap resampling for upscaling estimates

To quantify the sampling uncertainty in our national upscaling estimates, we adopted a stratified bootstrap resampling approach with 1,000 iterations and replacement within each crop type stratum. The point estimates reported in this study, including total Hg accumulation, source contributions, and fate allocations, were calculated directly from the original 301 field samples using the bottom-up mass balance framework described above. For each bootstrap iteration, we resampled the site-level data within each crop type stratum (wheat, rice, and maize), recalculated all relevant parameters, and recorded the results. The 2.5th and 97.5th percentiles of the bootstrap distributions were used to define the 95% confidence intervals (CIs). For source apportionment, we first obtained the atmospheric Hg contribution ratio ($f_{\text{air-veg}, k}$) for each crop at each isotopic sampling site using the two-endmember isotopic mixing model (Eq. 4). We then combined these site-level ratios with the crop-specific Hg accumulation masses obtained from each bootstrap iteration. By mass-weighting the contribution ratios, we yielded 1,000 estimates of the national-scale atmospheric contribution ratio ($f_{\text{air-veg, total}}$) via Eq. (6). The 2.5th and 97.5th percentiles of these estimates were taken as the 95% CI. For the fate allocation of crop Hg, we propagated the bootstrap uncertainty to each pathway-specific Hg estimate. In each of the 1,000 bootstrap iterations, we recalculated the total straw Hg mass for each crop ($\text{Straw}_{\text{Hg},k}$ in Eq. 7) from the resampled dataset, and then substituted this value into Eq. (8) to obtain a bootstrap estimate of $T_{l,\text{Hg},k}$ for each pathway l, while keeping the gridded pathway fractions

$r_{l,k}$ (p) fixed at their original values. This yielded 1,000 estimates of the Hg mass entering each fate pathway. The 95% CI for each pathway was determined by the 2.5th and 97.5th percentiles of the bootstrap distribution.

Data availability

Additional figures and tables can be found in the Supporting Information. Source data are provided with this paper and are also available on Figshare (https://figshare.com/s/8d96b10f5671f6b74ca6).

Code availability

The code associated with our analyses in this study is available on Code Ocean (https://doi.org/10.24433/CO.9051453.v2)[67].

References

1. *Ten chemicals of major public health concern* (WHO, 2020). https://www.who.int/news-room/photo-story/detail/10-chemicals-of-public-health-concern
2. *Global mercury assessment 2018* (UNEP, 2019). https://www.unep.org/resources/publication/global-mercury-assessment-2018
3. Mason, R.P. et al. Mercury biogeochemical cycling in the ocean and policy implications. *Environ. Res.* **119**, 101-117 (2012).
4. Outridge, P.M., Mason, R.P., Wang, F., Guerrero, S. & Heimbürger-Boavida, L.E. Updated global and oceanic mercury budgets for the united nations global mercury assessment 2018. *Environ. Sci. Technol.* **52**, 11466-11477 (2018).
5. Zhou, J., Obrist, D., Dastoor, A., Jiskra, M. & Ryjkov, A. Vegetation uptake of mercury and impacts on global cycling. *Nat. Rev. Earth Environ.* **2**, 269-284 (2021).
6. Sun, G. et al. Corn (*Zea mays* L.): a low methylmercury staple cereal source and an important biospheric sink of atmospheric mercury, and health risk assessment. *Environ. Int.* **131**, 104971 (2019).
7. Zhou, J. & Obrist, D. Global mercury assimilation by vegetation. *Environ. Sci. Technol.* **55**, 14245-14257 (2021).
8. Wang, X., Bao, Z., Lin, C.-J., Yuan, W. & Feng, X. Assessment of global mercury deposition through litterfall. *Environ. Sci. Technol.* **50**, 8548-8557 (2016).
9. Gruber, K. *Nature* **544**, S8-S10 (2017). https://doi.org/10.1038/544S8a.
10. Yin, R., Feng, X. & Meng, B. Stable mercury isotope variation in rice plants (*Oryza sativa* L.) from the Wanshan mercury mining district, SW China. *Environ. Sci. Technol.* **47**, 2238-2245 (2013).
11. Cui, L. et al. Accumulation and translocation of ^{198}Hg in four crop species. *Environ. Toxicol. Chem.* **33**, 334-340 (2014).
12. Zhu, Z., Wang, X., Wang, H., Lin, C. & Feng, X. Mercury exchange process between crop foliage and atmosphere by using single mercury isotope. *Environmental Chemistry* [in Chinese] **37**, 419-427 (2018).
13. Rai, P.K., Lee, S.S., Zhang, M., Tsang, Y.F. & Kim, K.-H. Heavy metals in food crops: Health risks, fate, mechanisms, and management. *Environ. Int.* **125**, 365-385

(2019).

14. Wang, D., Li, Z. & Wang, Q. Estimation of mercury uptake and distinction of corn cultivation in China. *Sci. Total Environ.* **906**, 167508 (2024).
15. Sun, T. et al. Use smaller size of straw to alleviate mercury methylation and accumulation induced by straw incorporation in paddy field. *J. Hazard. Mater.* **423**, 127002 (2022).
16. Xu, Z. et al. High-resolution atmospheric mercury emission from open biomass burning in China: Integration of localized emission factors and multi-source finer resolution remote sensing data. *Environ. Int.* **178**, 108102 (2023).
17. National Bureau of Statistics of the People's Republic of China. *China Statistical Yearbook 2025* [in Chinese] (China Statistics Press, 2025). https://www.stats.gov.cn/sj/ndsj/2025/indexch.htm
18. Kwon, S.Y., Selin, N.E., Giang, A., Karplus, V.J. & Zhang, D. Present and future mercury concentrations in Chinese rice: insights from modeling. *Global Biogeochem. Cycles* **32**, 437-462 (2018).
19. Tang, B., Chen, J., Wang, Z., Qin, P. & Zhang, X. Mercury accumulation response of rice plant (*Oryza sativa* L.) to elevated atmospheric mercury and carbon dioxide. *Ecotoxicol. Environ. Saf.* **224**, 112628 (2021).
20. Zhu, J., Wang, D. & Ma, M. Mercury release flux and its influencing factors at the air-water interface in paddy field in Chongqing, China. *Chin. Sci. Bull.* **58**, 266-274 (2013).
21. Zhao, B. et al. Prediction heavy metals accumulation risk in rice using machine learning and mapping pollution risk. *J. Hazard. Mater.* **448**, 130879 (2023).
22. Yang, A. et al. A review of mercury uptake, transport and bioaccumulation in rice. *Water Air Soil Pollut.* **234**, 377 (2023).
23. Cui, J. et al. Nitrogen cycles in global croplands altered by elevated CO_2. *Nat. Sustain.* **6**, 1166-1176 (2023).
24. Zhou, J. et al. Mercury fluxes, budgets, and pools in forest ecosystems of China: a review. *Crit. Rev. Environ. Sci. Technol.* **50**, 1411-1450 (2020).
25. Xu, Z., Wang, Z. & Zhang, X. Mapping the forest litterfall mercury deposition in China. *Sci. Total Environ.* **839**, 156288 (2022).

26. Zhang, L. et al. Updated emission inventories for speciated atmospheric mercury from anthropogenic sources in China. *Environ. Sci. Technol.* **49**, 3185-3194 (2015).
27. Chen, L. et al. Global distribution of mercury in foliage predicted by machine learning. *Environ. Sci. Technol.* **58**, 15629-15637 (2024).
28. Zhong, H. et al. Soil Geobacteraceae are the key predictors of neurotoxic methylmercury bioaccumulation in rice. *Nat. Food* **5**, 301-311 (2024).
29. Wang, X. et al. Evolving wastewater infrastructure paradigm to enhance harmony with nature. *Sci. Adv.* **4**, eaaq0210 (2018).
30. Zhang, H., Holmes, C.D. & Wu, S. Impacts of changes in climate, land use and land cover on atmospheric mercury. *Atmos. Environ.* **141**, 230-244 (2016).
31. Yuan, T. et al. Potential decoupling of CO_2 and Hg uptake process by global vegetation in the 21st century. *Nat. Commun.* **15**, 4490 (2024).
32. Xu, X. et al. Stomatal opening under high temperatures is controlled by the OST1-regulated TOT3–AHA1 module. *Nat. Plants* **11**, 105-117 (2025).
33. Liu, Y.-R. et al. Multidimensional drivers of mercury distribution in global surface soils: insights from a global standardized field survey. *Environ. Sci. Technol.* **57**, 12442-12452 (2023).
34. Wright, L.P. & Zhang, L. An approach estimating bidirectional air-surface exchange for gaseous elemental mercury at AMNet sites. *J. Adv. Model. Earth Syst.* **7**, 35-49 (2015).
35. Wang, S. et al. Light regulates stomatal development by modulating paracrine signaling from inner tissues. *Nat. Commun.* **12**, 3403 (2021).
36. Zhao, L., Meng, B. & Feng, X. Mercury methylation in rice paddy and accumulation in rice plant: a review. *Ecotoxicol. Environ. Saf.* **195**, 110462 (2020).
37. O'Connor, D. et al. Mercury speciation, transformation, and transportation in soils, atmospheric flux, and implications for risk management: a critical review. *Environ. Int.* **126**, 747-761 (2019).
38. Man, Y. et al. New insights into MeHg accumulation in rice (*Oryza sativa* L.): evidence from cysteine. *Environ. Sci. Technol.* **58**, 5942-5951 (2024).
39. Li, Y. F. et al. Organic selenium supplementation increases mercury excretion and decreases oxidative damage in long-term mercury-exposed residents from Wanshan,

China. *Environ. Sci. Technol.* **46**, 11313-11318 (2012).

40. Zhan, Z. et al. Forest mercury deposition observation in Chongqing: evaluating effectiveness of mercury pollution control over the past decade in southwestern China. *ACS ES&T Air* **2**, 286-294 (2025).

41. Fu, X. et al. Significant seasonal variations in isotopic composition of atmospheric total gaseous mercury at forest sites in China caused by vegetation and mercury sources. *Environ. Sci. Technol.* **53**, 13748-13756 (2019).

42. Wang, W. M., Ding, J. L., Shu, J. W. & Chen, W. Exploration of early rice farming in China. *Quat. Int.* **227**, 22-28 (2010).

43. Hu, B. et al. Current status, spatial features, health risks, and potential driving factors of soil heavy metal pollution in China at province level. *Environ. Pollut.* **266**, 114961 (2020).

44. Zhao, J., Li, N., Yang, X. & Sun, Z. For the protection of black soils. *Nat. Food* **6**, 119-120 (2025).

45. Wang, J., Zhang, Z. & Liu, Y. Spatial shifts in grain production increases in China and implications for food security. *Land Use Policy* **74**, 204-213 (2018).

46. Liu, M. et al. Rice life cycle-based global mercury biotransport and human methylmercury exposure. *Nat. Commun.* **10**, 5164 (2019).

47. Zhou, H. et al. Impacts of international food trade on methylmercury-related health risks. *Cell Rep. Sustain.* **2**, 100308 (2025).

48. Meng, M. et al. Accumulation of total mercury and methylmercury in rice plants collected from different mining areas in China. *Environ. Pollut.* **184**, 179-186 (2014).

49. Gan, C. et al. Maternal prenatal mercury exposure from rice and its association with newborn neurobehavioral development. *Environ. Pollut.* **390**, 127465 (2026).

50. Zhu, H., Zhong, H., Fu, F. & Zeng, Z. Incorporation of decomposed crop straw affects potential phytoavailability of mercury in a mining-contaminated farming soil. *Bull. Environ. Contam. Toxicol.* **95**, 254-259 (2015).

51. Islam, M.U., Guo, Z., Jiang, F. & Peng, X. Does straw return increase crop yield in the wheat-maize cropping system in China? A meta-analysis. *Field Crops Res.* **279**, 108447 (2022).

52. Cheng, J. et al. Strategies for crop straw management in China's major grain regions: yield-driven conditions and factors influencing the effectiveness of straw return. *Resour., Conserv. Recycl.* **212**, 107941 (2025).
53. Tang, W. et al. Increased methylmercury accumulation in rice after straw amendment. *Environ. Sci. Technol.* **53**, 6144-6153 (2019).
54. Yin, S. et al. Temporal and spatial dynamics of summer crop residue burning practices in North China: exploring the influence of climate change and anthropogenic factors. *Remote Sens.* **16**, 4763 (2024).
55. Feng, X. et al. Combating air pollution significantly reduced air mercury concentrations in China. *Natl. Sci. Rev.* **11**, nwae264 (2024).
56. Smerald, A., Rahimi, J. & Scheer, C. A global dataset for the production and usage of cereal residues in the period 1997–2021. *Sci. Data* **10**, 685 (2023).
57. Shi, W. et al. Quantifying reasonable straw removal rate to achieve food security, bioenergy transition and climate mitigation in China. *Resour. Conserv. Recycl.* **215,** 108114 (2025).
58. Franco, M.A. et al. How climate change and deforestation interact in the transformation of the Amazon rainforest. *Nat. Commun.* **16**, 7944 (2025).
59. Yuan, T. et al. Buffering effect of global vegetation on the air-land exchange of mercury: insights from a novel terrestrial mercury model based on CESM2-CLM5. *Environ. Int.* **174**, 107904 (2023).
60. Du, S., Wang, X., Zhou, Z., Zhang, T. & Ding, C. Kinetic characteristics of and critical stages for mercury accumulation in rice (*Oryza sativa* L.). *Ecotoxicol. Environ. Saf.* **258**, 114968 (2023).
61. Liu, N. et al. Mercury transport, transformation and accumulation recorded by stable isotopes during retreated glacier chronosequence of 250 years. *Environ. Sci. Technol.* **59**, 6085-6096 (2025).
62. Yu, B. et al. Isotopic composition of atmospheric mercury in China: new evidence for sources and transformation processes in air and in vegetation. *Environ. Sci. Technol.* **50**, 9262-9269 (2016).
63. Fu, X., Heimbürger, L.E. & Sonke, J.E. Collection of atmospheric gaseous mercury for stable isotope analysis using iodine- and chlorine-impregnated activated carbon

traps. *J. Anal. At. Spectrom.* **29**, 841 (2014).

64. Wang, X. et al. Global warming accelerates uptake of atmospheric mercury in regions experiencing glacier retreat. *Proc. Natl. Acad. Sci. U. S. A.* **117**, 2049-2055 (2020).

65. Wang, X. et al. Root uptake dominates mercury accumulation in permafrost plants of Qinghai-Tibet Plateau. *Commun. Earth Environ.* **3**, 287 (2022).

66. Hou, D. et al. Global soil pollution by toxic metals threatens agriculture and human health. *Science* **388**, 316-321 (2025).

67. Wang, Y.-K. et al. Staple crops as a key hub of biogeochemical mercury cycle across China. Code Ocean https://doi.org/10.24433/CO.9051453.v2 (2026).

Acknowledgements

We are grateful to P.-Y.G., Q.W. and R.W. for their assistance in sample measurements.

Funding statement

This research was supported by the National Natural Science Foundation of China (42425701), Guangdong Major Project of Basic Research (2025B0303000019), and Fundamental Research Funds for the Central Universities (2662025ZHPY007).

Author contributions

Y.-R.L. designed the study. Y.-K.W. carried out the field survey and lab analyses. N.L. conducted the isotope measurements. Y.-K.W., S.W., J.F., Y.-Y.H. analyzed the data. Y.-K.W. wrote the first draft of the paper. Y.-R.L., L.C., Y.Z., and X.W. revised the paper. All authors reviewed the paper and approved the final version of the manuscript.

Competing interests

The authors declare no competing interest.

Figure legends

Fig. 1 Mercury (Hg) accumulation in staple crop systems across China. A, B Mercury concentration in whole-plant staple crops and their paired soils; **C** Crop Hg accumulation per square meter; **D** Crop Hg accumulation at sampling sites and the estimated total amount of Hg accumulation in staple crops across China. Different lowercase letters in (A–C) indicate significant differences among crop types, as determined by one-way ANOVA followed by Tukey's HSD test ($p < 0.05$; n = 84 for wheat, 103 for rice, and 114 for maize). In panel D, circle size represents Hg accumulation per square meter, and color distinguishes different crops. Panels A–C show individual data points overlaid on boxplots. The central line marks the median, boxes cover the 25th–75th percentiles (IQR), whiskers span 1.5 × IQR, and points beyond whiskers denote outliers. Exact *p*-values and Source data are provided as a Source Data file.

Fig. 2 Effects of environmental variables on Hg accumulation in staple crops. A–C Relative importance of the top eight environmental variables for Hg accumulation in wheat, rice, and maize. Variable abbreviations: Biomass, crop biomass; LAI, leaf area index; Vcmax, maximum carboxylation rate; Soil Hg, soil mercury concentration; SOC, soil organic carbon; Soil TN, soil total nitrogen; MAT, mean annual temperature; SRAD, solar radiation; CO_2, atmospheric carbon dioxide concentration; Elev., Elevation; Hg^0_dep, elemental gaseous mercury deposition; Hg^{2+}_dep, divalent mercury deposition; Hg^{2+}_emis, divalent mercury emissions. Variables with importance > 5% are labeled, and the relative contributions of the five variable groups to crop Hg variation are shown on the right; different colours represent different variable groups. **D-F** Structural equation models showing the direct and indirect effects of geoclimatic factors, soil properties, vegetation parameters, anthropogenic factors, and Hg sources on Hg accumulation in wheat, rice, and maize. In the SEMs, G factors denote geoclimatic factors and A factors denote anthropogenic factors. Red and blue arrows indicate positive and negative effects, respectively, and standardized path coefficients are shown next to the arrows. Solid and gray dashed arrows indicate significant and non-significant paths, respectively. * indicates $p < 0.05$, ** indicates $p < 0.01$ and *** indicates $p < 0.001$. Exact *p*-values and Source data are provided as a Source Data file.

Fig. 3 Predicted spatial distribution of annual Hg accumulation in staple crops across China. A Wheat; **B** Rice; **C** Maize. Maps were generated using the extremely randomized trees (ERT) algorithm at 1-km resolution. Annual Hg accumulation was calculated as the sum of Hg loads across all crop tissues, where each tissue Hg load equals tissue-specific Hg concentration multiplied by corresponding tissue biomass. Values above each panel indicate the estimated total annual Hg accumulation for each crop, and the pie charts show the contribution of the dominant producing region. The identified hotspots for Hg accumulation were the North China Plain for wheat, the Jiangnan Hills for rice, and the Northeast China Plain for maize. Source data are provided as a Source Data file.

Fig. 4 Estimated fate of Hg accumulated in staple crops across China. A Mercury transferred to the food chain through grain consumption and livestock feed use; **B** Mercury retained in agricultural fields; **C** Mercury emitted to the atmosphere through open burning of crop residues; **D** Mercury allocated to other uses (e.g., household fuel and composting). Values shown in each panel indicate the estimated total annual Hg flux for the corresponding pathway. The map shading represents crop Hg accumulation capacity, with darker shades indicating higher Hg accumulation. Schematic illustrative icons of Figure 4 were sourced from BioRender (https://BioRender.com/kvk1g60). Source data are provided as a Source Data file.

Fig. 5 Staple croplands as active Hg transfer hubs: a conceptual diagram of Hg cycling and transfer pathways. Staple croplands transfer Hg to the food chain, atmosphere, and soil, whereas forests function primarily as net Hg sinks. Red arrows denote Hg outputs, whereas gray-white arrows denote Hg inputs. Figure 5 was created in BioRender (https://BioRender.com/e5jzbsm).

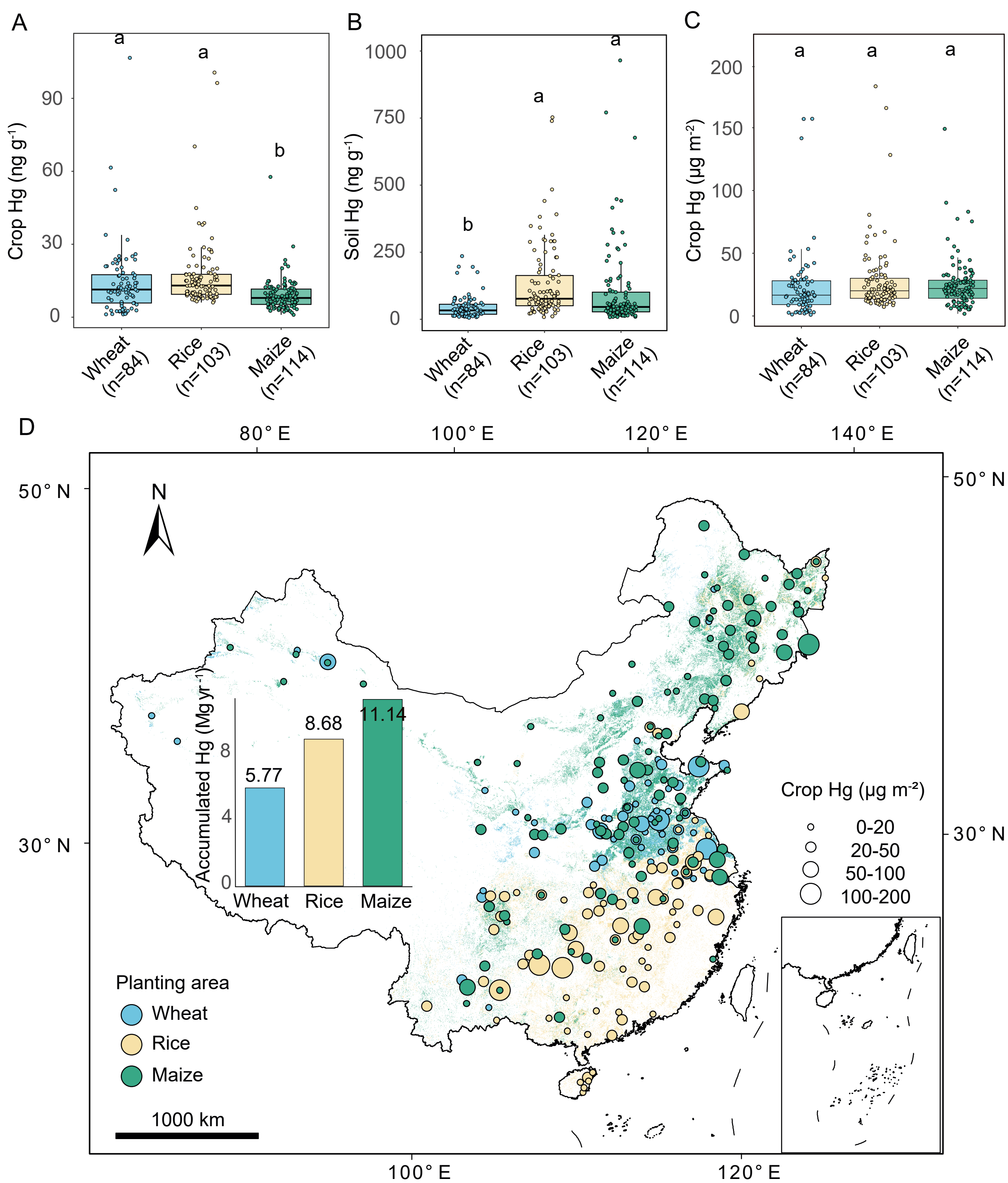

A
B
C
D
Crop Hg (ng g-1)
Soil Hg (ng g-1)
Crop Hg (μg m-2)
Wheat (n=84)
Rice (n=103)
Maize (n=114)
80° E
100° E
120° E
140° E
50° N
30° N
N
Accumulated Hg (Mg yr-1)
5.77
8.68
11.14
Wheat
Rice
Maize
Crop Hg (μg m-2)
0-20
20-50
50-100
100-200
Planting area
Wheat
Rice
Maize
1000 km

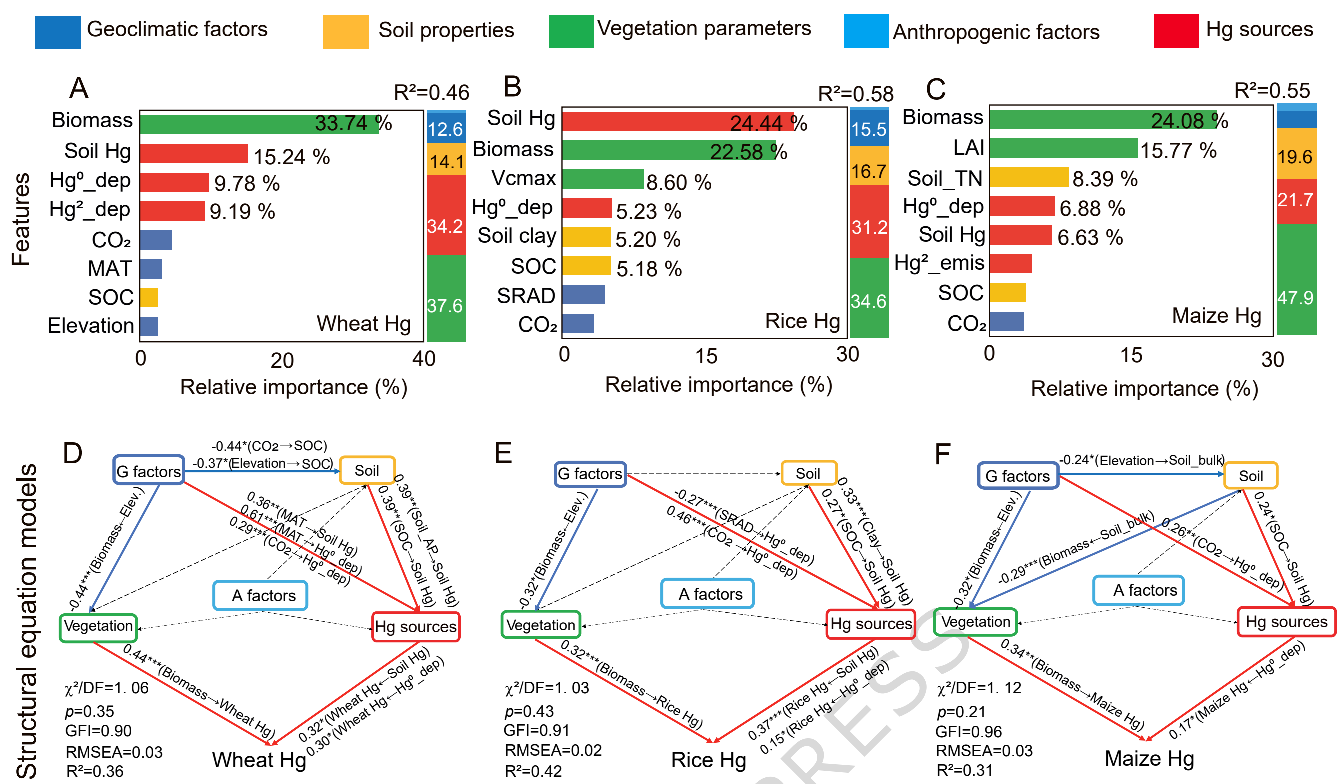

Geoclimatic factors
Soil properties
Vegetation parameters
Anthropogenic factors
Hg sources
A
R²=0.46
Biomass
Soil Hg
Hg⁰_dep
Hg²_dep
CO₂
MAT
SOC
Elevation
33.74 %
15.24 %
9.78 %
9.19 %
Wheat Hg
12.6
14.1
34.2
37.6
Features
0
20
40
Relative importance (%)
B
R²=0.58
Soil Hg
Biomass
Vcmax
Hg⁰_dep
Soil clay
SOC
SRAD
CO₂
24.44 %
22.58 %
8.60 %
5.23 %
5.20 %
5.18 %
Rice Hg
15.5
16.7
31.2
34.6
0
15
30
Relative importance (%)
C
R²=0.55
Biomass
LAI
Soil_TN
Hg⁰_dep
Soil Hg
Hg²_emis
SOC
CO₂
24.08 %
15.77 %
8.39 %
6.88 %
6.63 %
Maize Hg
19.6
21.7
47.9
0
15
30
Relative importance (%)
Structural equation models
D
G factors
Soil
A factors
Vegetation
Hg sources
Wheat Hg
-0.44*(CO2→SOC)
-0.37*(Elevation→SOC)
0.44***(Biomass←Elev.)
0.36**(MAT→Soil Hg)
0.61***(MAT→Hg⁰_dep)
0.29***(CO₂→Hg⁰_dep)
0.39**(Soil_AP→Soil Hg)
0.39**(SOC→Soil Hg)
0.44***(Biomass→Wheat Hg)
0.32*(Wheat Hg←Soil Hg)
0.30*(Wheat Hg←Hg⁰_dep)
χ²/DF=1. 06
p=0.35
GFI=0.90
RMSEA=0.03
R²=0.36
E
G factors
Soil
A factors
Vegetation
Hg sources
Rice Hg
0.32*(Biomass←Elev.)
-0.27***(SRAD→Hg⁰_dep)
0.46***(CO₂→Hg⁰_dep)
0.33***(Clay→Soil Hg)
0.27*(SOC→Soil Hg)
0.32***(Biomass→Rice Hg)
0.37***(Rice Hg←Soil Hg)
0.15*(Rice Hg←Hg⁰_dep)
χ²/DF=1. 03
p=0.43
GFI=0.91
RMSEA=0.02
R²=0.42
F
G factors
Soil
A factors
Vegetation
Hg sources
Maize Hg
-0.24*(Elevation→Soil_bulk)
0.32*(Biomass←Elev.)
-0.29***(Biomass←Soil_bulk)
0.26**(CO₂→Hg⁰_dep)
0.24*(SOC→Soil Hg)
0.34**(Biomass→Maize Hg)
0.17*(Maize Hg←Hg⁰_dep)
χ²/DF=1. 12
p=0.21
GFI=0.96
RMSEA=0.03
R²=0.31

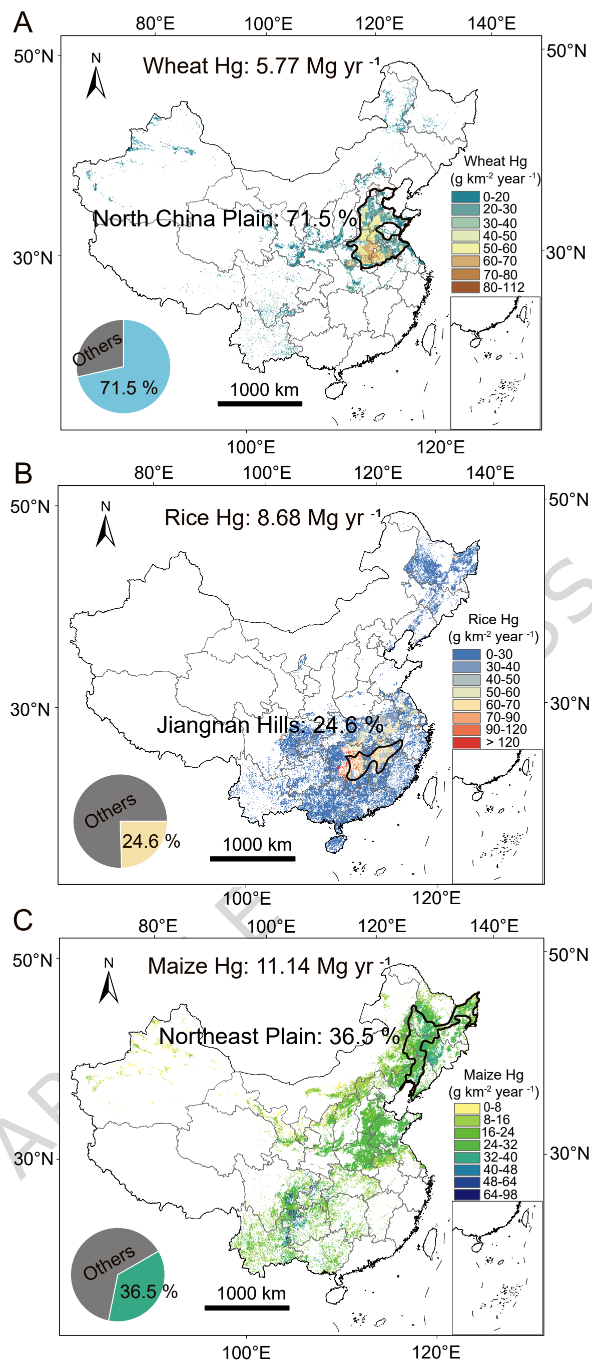
A
Wheat Hg: 5.77 Mg yr -1
North China Plain: 71.5 %
Wheat Hg
(g km-2 year -1)
0-20
20-30
30-40
40-50
50-60
60-70
70-80
80-112
Others
71.5 %
1000 km
B
Rice Hg: 8.68 Mg yr -1
Jiangnan Hills: 24.6 %
Rice Hg
(g km-2 year -1)
0-30
30-40
40-50
50-60
60-70
70-90
90-120
> 120
Others
24.6 %
1000 km
C
Maize Hg: 11.14 Mg yr -1
Northeast Plain: 36.5 %
Maize Hg
(g km-2 year -1)
0-8
8-16
16-24
24-32
32-40
40-48
48-64
64-98
Others
36.5 %
1000 km

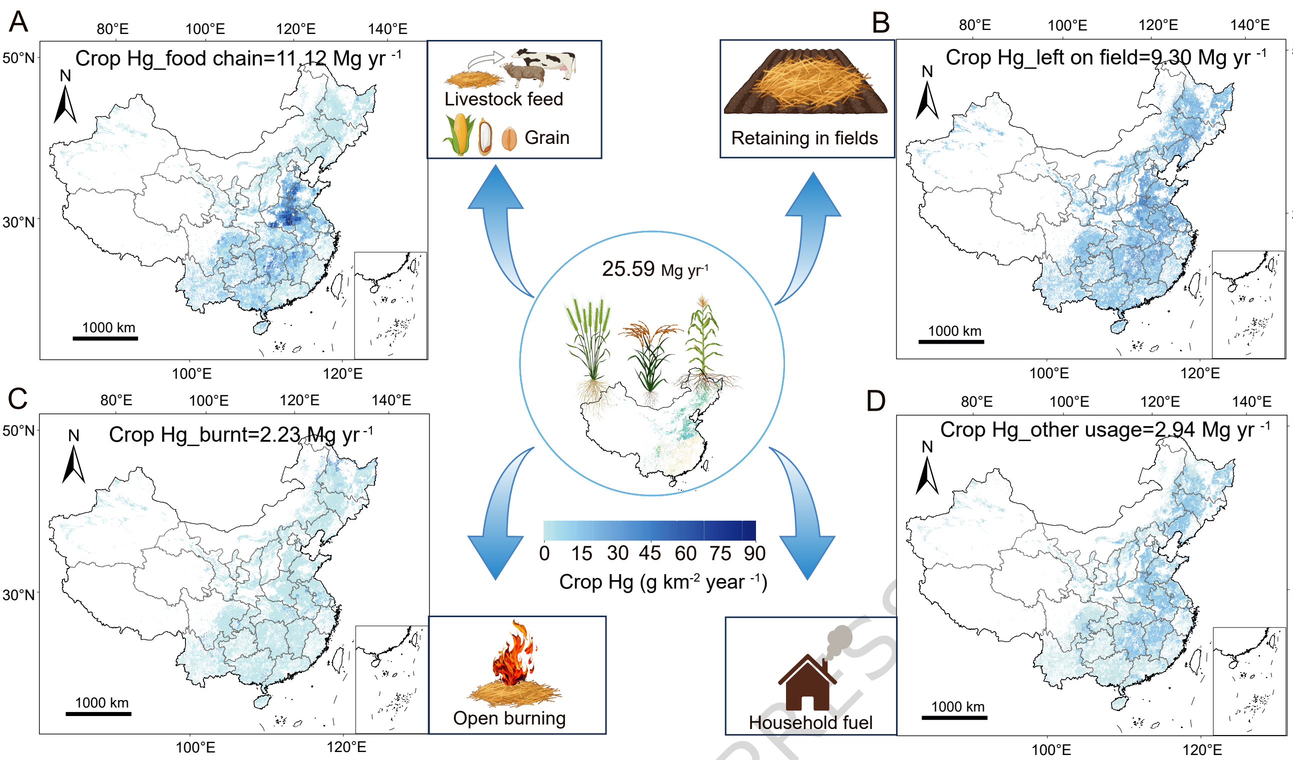
A
Crop Hg_food chain=11.12 Mg yr -1
Livestock feed
Grain
B
Crop Hg_left on field=9.30 Mg yr -1
Retaining in fields
25.59 Mg yr-1
C
Crop Hg_burnt=2.23 Mg yr -1
Open burning
D
Crop Hg_other usage=2.94 Mg yr -1
Household fuel
0 15 30 45 60 75 90
Crop Hg (g km-2 year -1)
1000 km
N
80°E 100°E 120°E 140°E
50°N 30°N

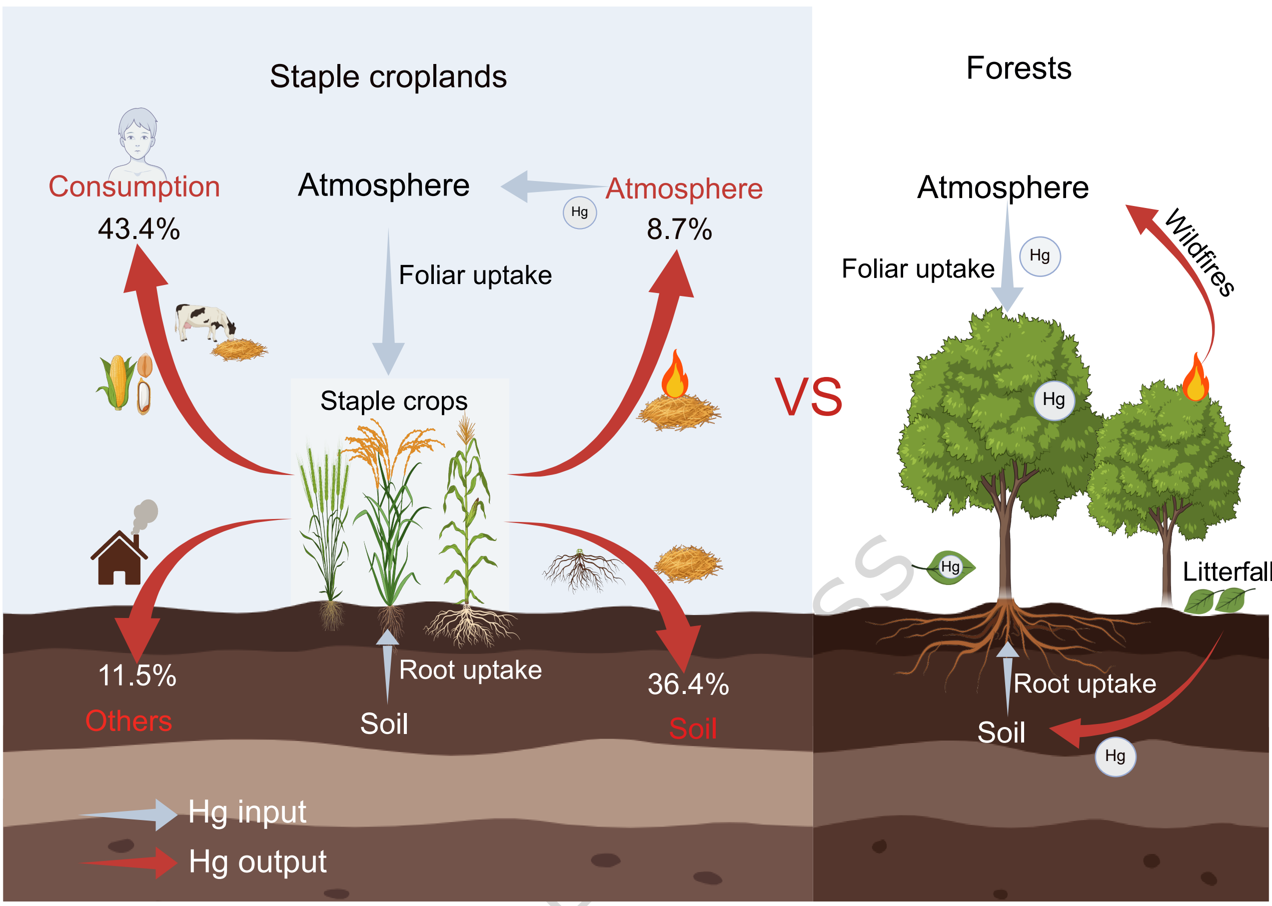

Staple croplands
Consumption
43.4%
Atmosphere
Atmosphere
8.7%
Hg
Foliar uptake
Staple crops
11.5%
Others
Root uptake
Soil
36.4%
Soil
Hg input
Hg output
VS
Forests
Atmosphere
Foliar uptake
Hg
Wildfires
Hg
Hg
Litterfall
Root uptake
Soil
Hg